FEMS Microbiology Ecology, 2025, **101**, fiae158
DOI: 10.1093/femsec/fiae158
Advance access publication date: 17 February 2025
Research Article

Temperature-induced changes in the relevance of viral lysis and microzooplankton grazing of Antarctic phytoplankton indicates future alterations in seasonal carbon flow

Tristan E.G. Biggs [1,2,*], Gonçalo J. Piedade[1,2], Ella M. Wesdorp[1,2], Michael P. Meredith[3], Claire Evans[4], Corina P.D. Brussaard[1,2,*]

[1]Department of Marine Microbiology and Biogeochemistry, NIOZ Royal Netherlands Institute for Sea Research, 1797 SZ, Texel, The Netherlands
[2]Department of Freshwater and Marine Ecology, Institute for Biodiversity and Ecosystem Dynamics (IBED), University of Amsterdam, 1098 XH, Amsterdam, The Netherlands
[3]British Antarctic Survey, Natural Environmental Research Council, CB3 0ET, Cambridge, United Kingdom
[4]Ocean BioGeosciences, National Oceanography Centre, SO14 3ZH, Southampton, United Kingdom
*Corresponding authors. Tristan E.G.Biggs and Corina P.D.Brussaard, Department of Marine Microbiology and Biogeochemistry, NIOZ Royal Netherlands Institute for Sea Research, 1797 SZ, Texel, The Netherlands. E-mails: tristan.biggs@nioz.nl; corina.brussaard@nioz.nl
Editor: [Martin Hahn]

Abstract

Phytoplankton play a pivotal role as the primary producers in polar marine ecosystems. Despite evidence suggesting that production rates and loss factors vary from year to year, and thus drive dynamic ecosystem functioning, interannual comparisons remain sparse. In this study, we examined viral lysis and microzooplankton grazing rates on Antarctic phytoplankton during two productive seasons and compared them with published data from a previous year. Higher rates of phytoplankton gross growth and total mortality during the warmer productive season suggest global warming induced increases in the magnitude of ecosystem carbon flow. Viral lysis rates appear to be relatively independent of average seasonal temperatures, whereas grazing rates were lower during the colder productive seasons (average temperature <0°C). This resulted in a greater relative impact of viral lysis on phytoplankton mortality, particularly pronounced during periods of phytoplankton accumulation. The interannual variations in phytoplankton fate are likely due to a stronger coupling between rates of viral infection and phytoplankton growth compared with grazing. Our results emphasize the importance of monitoring rates of viral lysis, specifically in combination with the size and taxonomy of the phytoplankton community. Collectively these factors determine the relative significance of the different carbon fates, and hence the ocean's efficacy as a carbon sink.

Keywords: Antarctic phytoplankton; grazers; growth; marine viruses; seasonal mass balance; temperature

Introduction

The Southern Ocean exhibits pronounced environmental variability across seasonal and interannual time scales, characterized by fluctuations in parameters such as temperature, micronutrient concentrations, and light availability. These variations exert significant influence on the dynamics of phytoplankton populations, encompassing both production and losses, as well as shaping community composition (Edwards et al. 2016, Biggs et al. 2022, Krumhardt et al. 2022). Given that phytoplankton serve as the foundational tropic level in marine pelagic ecosystems, the ramifications of this variability extend to the transfer of energy and matter to higher trophic levels, as well as the sequestration of carbon to the deep ocean. As the Southern Ocean is a net sink for atmospheric CO_2, it's phytoplankton photosynthetic outputs likely play an important role in the sequestration of organic carbon through mechanisms such as the biological and microbial carbon pumps (DeVries et al. 2012, Nowicki et al. 2022).

While grazing has traditionally been considered the primary pathway governing the fate of Antarctic phytoplankton cells (Le Quéré et al. 2016, Rohr et al. 2017, Irion et al. 2021, Kauko et al. 2021), recent findings have highlighted the substantial contribution of viral lysis to phytoplankton losses across key taxonomic groups (Biggs et al. 2021, Eich et al. 2022). Grazing channels organic carbon and nutrients towards higher trophic levels, whereas viral lysis diverts primary production away from zooplankton, redirecting it towards the dissolved organic matter pool. This shift reduces the efficiency of the biological carbon pump (Brussaard et al. 2005a,b, Suttle 2007, Weitz and Wilhelm 2012 , Lønborg et al. 2013, Mojica et al. 2016). Notably, viral infection of diatoms may induce aggregation and sedimentation, suggesting that viruses could serve as an alternative mechanism for carbon export (Yamada et al. 2018) with consequences for the elemental stoichiometry of sinking material (Brussaard et al. 2008). Beyond their biogeochemical impact, lytic viruses significantly influence phytoplankton community composition and species succession due to their typically high host-specificity (Brussaard and Martínez 2008, Nagasaki 2008, Mojica and Brussaard 2014). To model variability in planktonic community structure and carbon cycling more accurately, a better understanding of viral lysis dynamics and its connection to phytoplankton growth and mortality is required.

Received 28 February 2024; **revised** 26 September 2024; **accepted** 14 February 2025

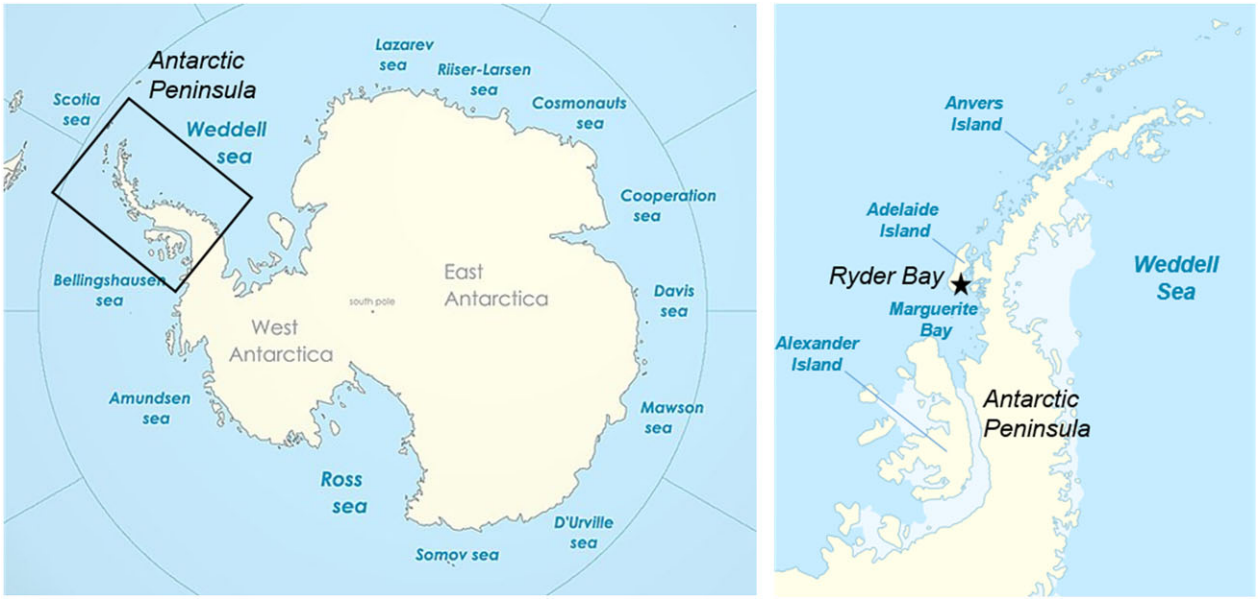

Figure 1. Map of the study site: (left) large scale map of Antarctica showing the location of the Antarctic Peninsula and surrounding seas, (right) the location of Ryder Bay in northern Marguerite Bay to the east of Adelaide Island and to the west of the Antarctic Peninsula.

The coastal waters along the Western Antarctic Peninsula (WAP) are highly productive (Vernet et al. 2008) and serve as a model study area to better understand the impact of environmental change on polar food web functioning (Schofield et al. 2018). Annual variations in chlorophyll *a* (Chl-*a*) concentrations (Venables et al. 2023), the phytoplankton community (Venables et al. 2013, Rozema et al. 2017b) and, particularly in virioplankton abundances (Evans et al. 2017), suggest potential variations in viral lysis rates. Additionally, the influence of global warming on shifting the dominance from micro-sized diatoms to nano-sized phytoplankton (Rozema et al. 2017b) underscores the importance of phytoplankton size classes, which not only dictate the size class of zooplankton grazing, but also determine the amount of organic carbon shunted by viruses to the microbial food web. Given that the cumulative balance of production and losses over a seasonal cycle determines the ecosystem's carrying capacity (Sarker and Wiltshire 2017), it is critical to assess the importance of viral lysis consistently and explore potential interannual differences.

Antarctic waters exhibit a productive period commencing in spring/early summer, driven by a seasonal reduction in wind speed that initiates a shallowing of the mixed layer depth, enhanced light availability and a gradual rise in surface temperatures. Despite peak summer water temperatures often reaching 1°C–2°C, interannual variation between productive seasons (November–April) can result from substantial differences in forcing and water column dynamics (Meredith et al. 2013, Venables et al. 2013). These variations influence the timing and extent of the phytoplankton productive cycle (for example peak seasonal Chl-*a* concentrations can range from <5 to >25 μg l^{-1}; Rozema et al. 2017b) with implications for carbon cycling. Given that temperature can directly affect metabolic rates, a comprehensive multi-year assessment of growth, viral lysis, and grazing rates for the different phytoplankton populations is essential to understand seasonal dynamics and interannual differences.

In this study, we investigate growth, viral lysis and microzooplankton grazing rates of Antarctic coastal phytoplankton during two relatively colder productive seasons (average temperature at sampling depth <0°C; Venables and Meredith 2014, van Leeuwe et al. 2020) and compare them with rates determined during a relatively warmer year (average temperature >0°C at the same sampling site; Biggs et al. 2021).

Materials and methods

Study location and sampling

Seawater for the experiments was collected alongside the year-round sampling programme at the Rothera Time Series site (RaTS, latitude 67.572° S; longitude 68.231° W; Clarke et al. 2008) in Ryder Bay on the WAP (Fig. 1). Sampling was performed during the Austral summer from November to February in 2012–2013, 2013–2014, and 2018–2019. Discrete seawater samples were collected from a depth of 15 m by a 12-l Niskin bottle deployed from a small boat. Full water column profiles were obtained using a SeaBird 19+ conductivity temperature depth instrument supplemented with a LiCor photosynthetically available radiation (PAR) and an in-line fluorescence sensor (WetLabs). Seawater samples were shielded from light and processed directly upon return to the research base in a temperature-controlled lab maintained at close to *in situ* temperature (~0.5°C). Modified dilution mortality assay experiments were conducted to examine phytoplankton growth, grazing, and mortality rates, approximately once per week depending on weather conditions.

Chl-*a*

Samples for Chl-*a* concentration were obtained by filtering 1–4 l through GF/F glass fiber filters (47 mm, Whatman, The Netherlands). Filters were wrapped in aluminium-foil, snap-frozen in liquid nitrogen and stored at −80°C until analysis. Chl-*a* concentrations were analysed by high performance liquid chromatography (HPLC). For 2012–2013 and 2013–2014 seasons, Chl-*a* were analysed according to Brussaard et al. (2016). For the 2018–2019 season, filters were freeze dried (48 h) and pigments extracted using 90% acetone (48 h at 4°C in the dark; van Leeuwe et al. 2006). Pigments were separated by HPLC (Waters model 2690), equipped with a 3.5-μm particle size Zorbax Eclipse XDB-C8 column with a cooled autosampler (4°C) according to Van Heukelem and Thomas (2001). Pigment detection and quantification was based on

comparison with DHI LAB standards (DHI, Hørsholm, Denmark). Chl-*a* concentrations were converted to cellular carbon (Chl-C) using taxon-specific conversion factors according to Garibotti et al. (2003), with the exception of Dinophyceae for which we used an average of ratios by Llewellyn et al. (2005) and Agirbas et al. (2015).

Phytoplankton abundance, growth, and losses

For phytoplankton enumeration, fresh 3.5 ml subsamples were analysed using flow cytometry according to Marie et al (1999). A Becton Dickinson (BD) FACSCalibur was used for sample analysis in 2013–2014, whereas a BD FACSCelesta was used during the 2018–2019 campaign. Both were equipped with an air-cooled Argon laser with an excitation wavelength of 488 nm (15 mW) and the trigger set on red fluorescence. Phytoplankton populations were distinguished using bivariate scatter plots of red Chl-*a* autofluorescence versus side scatter (Fig. S1). Average cell diameter of the different phytoplankton populations was estimated using size fractionation (Biggs et al. 2019). The 17 phytoplankton populations had average cell diameters between 0.9 and 20 µm, of which Phyto 1–3 ranged between 1 and 3 µm average cell diameter, Phyto 4–13 were ≤10 um and Phyto 14–17 ranged between 11 and 20 µm. Phyto 6, 7, 10, and 11 were discriminated as cryptophytes based on their orange phycoerythrin autofluorescence (Fig. S1; Li and Dickie 2001), Phyto 3 was identified as *Phaeocystis* spp., and Phyto 8, 9, and 12–17 were diatoms based on microscopic identification and/or taxonomic identification (Biggs et al. 2019). For interoperability of flow cytometry vocabulary as suggested by Thyssen et al. (2022), the phytoplankton groups identified in this study could be placed into three 'common' categories: RedPico (Phyto 1–3), RedNano (Phyto 4, 5, 8, 9, and 12–17), and OraNano (Phyto 6, 7, 10, and 11).

The cellular carbon (C) content of each phytoplankton population was estimated from the average cell diameter and using conversion factors of 237 and 196.5 fg C μm^{-3} for pico- and nano-sized phytoplankton populations, respectively (Garrison et al. 2000, Worden et al. 2004). For phytoplankton growth and losses, rates were first converted into cells and integrated over time, then to cellular C according to Biggs et al. (2021).

The modified dilution assay was used to determine viral lysis and grazing rates of the identified phytoplankton populations according to Biggs et al. (2021). This method provides direct measurements of viral lysis and grazing rates concomitantly. To accommodate a diel cycle (necessary for phytoplankton synchronized cell division, as well as for viral infection dynamics), we incubated 24 h. We recommend gentle handling of the samples (e.g. siphoning the sample into the bottles), preparing at *in situ* temperature and dimmed light, no air bubbles in the incubation bottles, and preferably fresh counting of the phytoplankton samples. The modified dilution method has (as any method) its limitations and we refer to the literature for more specifics (Evans et al. 2003, Baudoux et al. 2006, 2007, Kimmance et al. 2007, Kimmance and Brussaard 2010). In short, <200 µm-sieved natural seawater was gently siphoned into 1-l polycarbonate bottles with either grazer-free (0.45 µm) or grazer + virus free (30 kDa) filtrates to create a dilution series (in triplicate) of 100%, 70%, 40%, and 20% seawater. A grazer-free diluent was prepared by gravity filtration of natural seawater using a 0.45-µm Sartopore capsule filter with a 0.8-µm prefilter (Sartopore 2300, Sartorius Stedim Biotech, Göttingen, Germany). The grazer + virus free ultrafiltrate (30 kDa) was created by tangential flow filtration of natural seawater using a polyethersulfone membrane (Vivaflow 200, Sartorius Stedim Biotech). The incubation bottles were transferred (protected from light) to an outdoor (natural seawater) flow-through incubator and randomly placed on a slow-turning wheel (~0.5 r m^{-1}) and incubated for 24 h at *in situ* temperature and light conditions (using neutral-density mesh).

Phytoplankton enumeration was performed by flow cytometric analysis of live samples (10 min on high flow rate with an average analysed volume of ~1 ml) at the beginning (T_0) and end (T_{24}) of each experiment. Actual dilutions (at T_0) were calculated for each incubation bottle as a proportion of the 100% replicates average in each series. Apparent growth rates for each phytoplankton population were calculated using the natural logarithm, and plotted against dilution. Subsequently, grazing rates were obtained from the slope of the linear regression in the 0.45-µm dilution (grazer free) series and total mortality (M_{tot}) as the slope in the 30 kDa (grazer + virus free) series. Rates of viral lysis were calculated by subtraction (M_{tot} minus grazing). In cases where we consider the analyses as failed, i.e. where the slope of the linear regression was positive and >0.1 (Kimmance et al. 2007), we considered that proper estimation of the grazing and viral lysis rates failed and the values were discarded ($n = 36$). Gross growth rates (μ_{gross}) were represented by the *y*-axis intercept of the linear regression. When the apparent growth rates of the 20% dilution series were equal to or lower than growth rates of the 40% dilution series, the 20% values were removed as this indicates phytoplankton growth limitation. Similarly, when the phytoplankton growth rates of the 70% dilution series were equal to those of the 100% series, the latter were removed as this indicates predator (grazers, viruses) concentrations were not diluted enough to allow an observable increase in apparent growth rates.

In the case of missing replicates (e.g. due to technical error during the assay or flow cytometric analysis) or clear outliers (compared to the series, often when population abundance was very low), we performed the regression analysis without those values. Although there is not a specific threshold concentration for the application of the dilution method, based on the numbers enumerated during flow cytometry analysis, most analyses that were discarded had a low cell concentration (<100 ml^{-1}) in combination with high variation.

For interannual comparison, the obtained phytoplankton growth and loss rates from November 2013–February 2014 and November 2018–February 2019 were compared to published rates from December 2012 to March 2013 (Biggs et al. 2021). Approaches and analysis of data were the same for the 3 years.

Statistics

A significant difference between the regression coefficient of the 0.45-µm series and zero indicates significant grazing whilst that of the 30-kDa series indicates both significant μ_{gross} and M_{tot}. A significant difference between the regression coefficients of grazing and M_{tot} (as tested by analysis of covariance, $P < .10$, using R statistical software; R Development Core Team 2023) represents significant rates of viral lysis.

Throughout the text, values are quoted with their respective standard deviations (i.e. $\pm 1\sigma$). Differences between environmental variables, as well as between μ_{gross}, grazing, viral lysis, and M_{tot} rates (also cells and carbon), were tested using either a two-tailed Student's or Welch's *t*-test and a Mann–Whitney U Test if data deviated from normality as assessed by the Shapiro–Wilk test (SigmaPlot v14, from Systat Software, Inc., San Jose California, USA). The strength of relationships between viral lysis, grazing, and gross growth were determined using a Pearson's correlation test (SigmaPlot v14).

Model of phytoplankton carbon flow

To model phytoplankton carbon flow, we need to calculate daily amounts of carbon produced by phytoplankton production and lost by grazing and viral lysis using the equations presented in Biggs et al. (2021):

The total amount of phytoplankton carbon produced over a time interval of T days (P_T) can be calculated by integrating the production rate over time:

$$P_T = \frac{\mu gross}{\mu gross - m_{tot}} \left(X_0 \, e^{\left(\mu gross - m_{tot}\right)T} - X_0 \right),$$

where X is the minimum phytoplankton carbon concentration at the start of the time period ($_0$), μ_{gross} is the gross specific growth rate, and m_{tot} is the total specific mortality rate driven by viral lysis (m_V) and grazing (m_G; i.e. $m_{tot} = m_V + m_G$).

Similarly, the total amount of phytoplankton carbon lost over T days (L_T) can be calculated as follows:

$$L_T = \frac{m_{tot}}{\mu gross - m_{tot}} \left(X_0 \, e^{\left(\mu gross - m_{tot}\right)T} - X_0 \right).$$

This total loss is partly due to viruses and partly to grazers. Specifically, the total amount of phytoplankton carbon lost over T days by viral lysis is $(m_V/m_{tot})L_T$ and by grazing is $(m_G/m_{tot})L_T$. We calculated daily rates, with a time interval of $T = 1$ day, in line with the 24-h incubation period used in the dilution assays. Using the average rates from the accumulation and decline phases (identified in Fig. 8), the net change in phytoplankton standing stock ($P_T - L_T$) per day is added (during accumulation) or subtracted (during decline) to standing stock from the previous day until the maximum or minimum values are attained. The minimum and maximum standing stock carbon values used are those observed in each season.

Results

Physicochemical data

Among the environmental variables considered (Tables S1–S3), temperature exhibited the most pronounced variation across the different years (Fig. 2). The productive seasons of 2013/2014 and 2018/2019 were characterized by comparatively lower summer temperatures (Fig. 2) and were designated as cold productive seasons 1 and 2 (CPS1 and CPS2, respectively). In contrast, the 2012/2013 season was designated as the relatively warm productive season (WPS). Analysis revealed a statistically significant difference in the average seawater temperature on days when the experiments were conducted, with CPS1 (−0.37°C) and CPS2 (−0.42°C) displaying significantly lower temperatures compared to WPS (0.37 °C; $P = .0229$ and .0145, respectively; Tables S1–S3). However, temperature did not significantly differ between the two colder seasons CPS1 and CPS2 ($P = .828$). Long-term temperature records for the productive seasons in the preceding decade (Fig. 3) corroborated the classification of CPS1 and CPS2 as relatively cold and WPS as relatively warm (Fig. 3). Notably, temperatures in CPS1 and CPS2 only exceeded 0°C in early to mid-January (Fig. 2), coinciding with a more pronounced decline in salinity compared to WPS (Fig. S2A). This led to a sustained period of heightened water column stratification in CPS1 and CPS2, extending beyond that observed in WPS (Fig. S2B). Average PAR levels were notably higher in CPS2 than in CPS1 and WPS, with values of 107 µmol quanta m^{-2} s^{-1} compared to 51 µmol quanta m^{-2} s^{-1} and 34 µmol quanta m^{-2} s^{-1}, respectively. This difference mainly arose due to elevated PAR

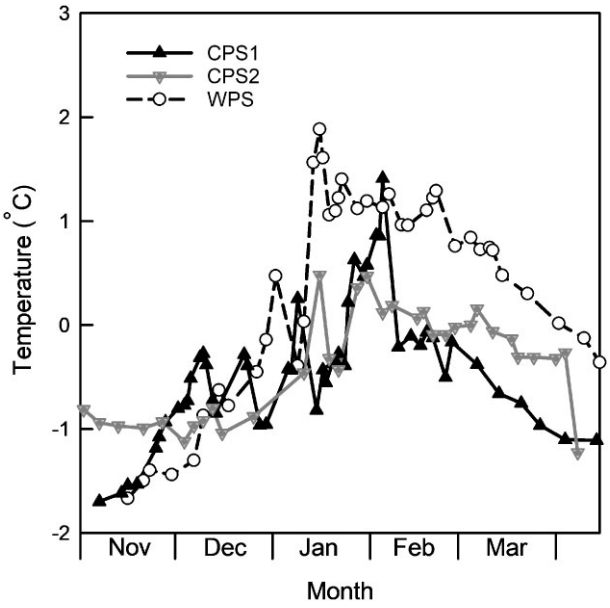

Figure 2. Temperature dynamics at the sampling site (15 m depth) during the cold productive seasons of 2013/2014 (CPS1) and 2018/2019 (CPS2), as well as the WPS of 2012/2013.

levels during the initial half of December in CPS2 (Fig. S2C). Nutrient concentrations rapidly decreased during these prolonged stratification periods. Potentially limiting concentrations of dissolved inorganic phosphate and nitrate were recorded only for brief intervals at the onset of February in CPS1, the end of January in CPS2, and the beginning of January and mid-March for WPS (Tables S1–S3).

Chl-*a* and phytoplankton abundance

The average Chl-*a* concentration for the colder CPS1 and CPS2 was 2.7 µg l^{-1} and 2.4 µg l^{-1}, respectively (Fig. 4), which is 1.6-fold and 1.8-fold lower, respectively, than the Chl-*a* concentration observed in WPS (4.3 µg l^{-1}). In contrast to WPS, both CPS1 and CPS2 exhibited a singular phytoplankton bloom without an additional late summer bloom (Fig. 4). Nevertheless, the ≤ 20 µm size fraction comprised largely comparable shares, i.e. 67% (of total Chl-*a*) in CPS1, 57% in CPS2, and 70% in WPS (Fig. 4).

The average total phytoplankton abundance was lowest in CPS1 at 3 700 cells ml^{-1} compared to 6200 cells ml^{-1} in CPS2 and 5500 cells ml^{-1} in WPS. The Phyto 1–3 populations dominated abundances (Fig. S3) at the onset of all seasons, accounting for 68%–90% of the total in November when Chl-*a* concentrations were low (Fig. 4). Among these, *Phaeocystis* Phyto 3 was the most prevalent group during both cold seasons CPS1 and CPS2, constituting an average of 42% and 41%, respectively, compared to 16% in WPS (Fig. S3). Diatoms Phyto 8, blooming from January to March, were most prominent in WPS (24%), while they represented only 4% in CPS1 and were not observed in CPS2. Conversely, similar-sized diatoms Phyto 9 (4.5–7 µm diameter) played a significant role during the cold productive seasons, contributing 26% in CPS1 from December to January and 16% between the end of January and the end of February in CPS2 (Fig. S3). Notable differences between the colder and warmer seasons were also observed for many of the other phytoplankton populations. Cryptophytes Phyto 6 and diatoms Phyto 8 and 14 were more abundant during WPS (297 ml^{-1}, 1759 ml^{-1}, and 696 ml^{-1}, respectively) compared to CPS1 (109, 250, and 238 ml^{-1}) and CPS2

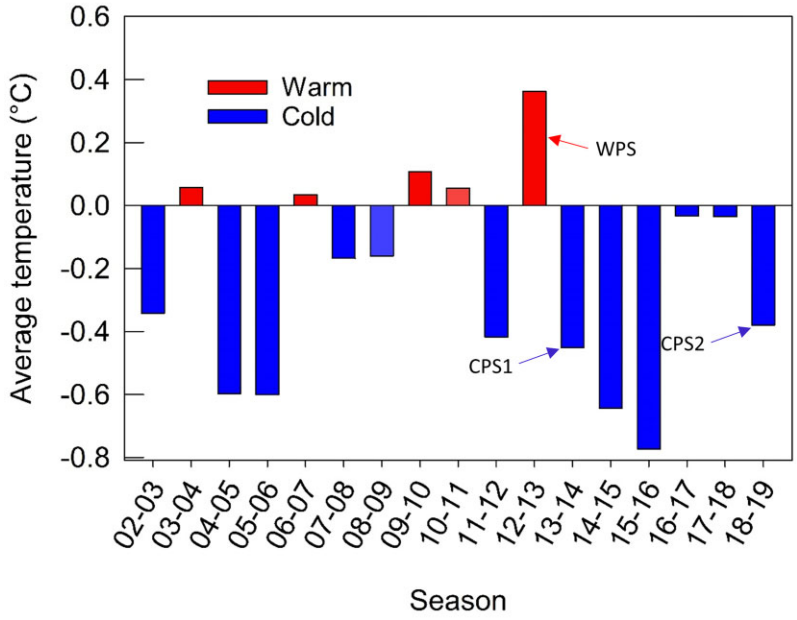

Figure 3. Average seawater temperature at the sampling site during each productive season (15 m depth between 1 November and 15 April) in Ryder Bay from 2002 to 2019 (02–19). Average temperatures above and below 0°C are defined as relatively warm and cold productive seasons, respectively. The seasons in this study are indicated by arrows.

(147, 0, and 206 ml^{-1}). Conversely, *Phaeocystis* Phyto 3 and diatom Phyto 9 exhibited much higher abundances in both cold seasons than in WPS (CPS1: 1597 ml^{-1} and 677 ml^{-1}; CPS2: 3429 ml^{-1} and 324 ml^{-1}; WPS: 1059 ml^{-1} and 188 ml^{-1}, respectively). Furthermore, the large-sized (20 µm) diatom Phyto 17 was mainly observed in CPS1 and CPS2 (72 ml^{-1} and 58 ml^{-1}, respectively), in contrast to its low abundance (1 ml^{-1}) in WPS.

When converted to phytoplankton carbon content, *Phaeocystis* Phyto 3 contributed 20% of the total in CPS2, followed by Phyto 4, 9, 14, and 17 accounting for 13%, 13%, 8%, and 12% of total algal carbon, respectively. In CPS1, *Phaeocystis* contributed only 12%, with Phyto 14 and Phyto 17 dominating total carbon content at 19% and 34%, respectively. In WPS, the diatoms Phyto 8 and Phyto 14 were the major contributors, constituting 20% and 41%, respectively, of total phytoplankton carbon. Phyto 17 was the dominant phytoplankton group indicative for the colder CPS1 and CPS2, while it was Phyto 8 for the warmer WPS.

Temperature related trends in viral lysis and grazing rates

During the colder seasons of CPS1 and CPS2, the mean specific viral lysis rates of the various different phytoplankton populations (Tables S4–S6) were slightly higher overall than rates of grazing (CPS1: 0.21 versus 0.18 d^{-1}, $n = 61$, and CPS2: 0.18 versus 0.16 d^{-1}, $n = 59$, respectively), with a significant difference for CPS1 ($P = .035$). Conversely, in WPS, the average rate of viral lysis was slightly lower and not significantly different from grazing (0.29 versus 0.31 d^{-1}, respectively, $n = 98$). Interannual comparison reveals the specific grazing rates to be significantly 1.7 and 1.9-fold lower for both cold seasons of CPS1 ($P < .001$) and CPS2 ($P < .001$) compared to WPS. However, viral lysis rates were not significantly different between the seasons. When focusing solely on the phytoplankton populations with the highest rate measurements across all seasons (i.e. Phyto 1, 3, and 9; $n \geq 8$ in each season), the trend remained consistent. Average grazing rates in CPS1 (0.14 d^{-1}, $n = 28$) and CPS2 (0.15 d^{-1}, $n = 33$) were significantly lower compared to WPS (0.32 d^{-1}, $n = 43$; $P = .004$ and .009 respectively), while viral lysis rates were not significantly different (CPS1 = 0.24 d^{-1}; CPS2 = 0.20 d^{-1}; WPS = 0.27 d^{-1}). A similar trend persisted when examining these phytoplankton populations only during matching time periods (i.e. December–February; grazing of Phyto 1, 3, and 9 = 0.11 d^{-1}, 0.18 d^{-1}, and 0.33 d^{-1}; viral lysis = 0.25 d^{-1}, 0.18 d^{-1}, and 0.27 d^{-1}; $n = 23$, 26, and 38, respectively). Despite lower average grazing rates in CPS1 and CPS2 compared to WPS, a negative correlation between viral lysis and grazing was consistently observed across all seasons (Pearson's $r = -0.231$, $n = 218$, $P < .001$, Fig. 5).

Analogous to grazing, average rates of phytoplankton gross growth were significantly 1.7-fold lower in the colder seasons (0.35 d^{-1} for CPS1 and CPS2) compared to WPS (0.61 d^{-1}; $P < .001$ for both). For a more detailed examination of the influence of temperature, gross growth rates were plotted against grazing and viral lysis with data from both cold seasons combined (i.e. CPS1 + CPS2 and WPS; Fig. 6). For CPS1 + CPS2, a significant relationship was observed for both grazing ($P = .0397$) and viral lysis ($P < .0001$), as was also observed for WPS (grazing $P = .0026$, viral lysis $P = .0002$). However, a steeper slope for the CPS1 + CPS2 lysis rate regression (0.29) compared to grazing (0.13) indicates that viral lysis rates increase faster than grazing (in relation to gross growth) during the cold productive seasons. This is in contrast to WPS, where the grazing and viral lysis regression slopes were more similar (0.26 and 0.35 respectively; Fig. 6).

General and temperature-related trends in the share of viral lysis

Plotting total mortality versus gross growth rates revealed a consistent pattern across all seasons, wherein higher gross growth rates coincided with increased mortality ($P = .0135$, $< .001$, and $< .001$, respectively; Fig. 7). The shallower linear regression slope for CPS1 (0.30) and CPS2 (0.51) compared to closer coupling of gross growth and losses for WPS (0.61; Fig. 7) implies lower rates of growth were required to outgrow losses and obtain an increase

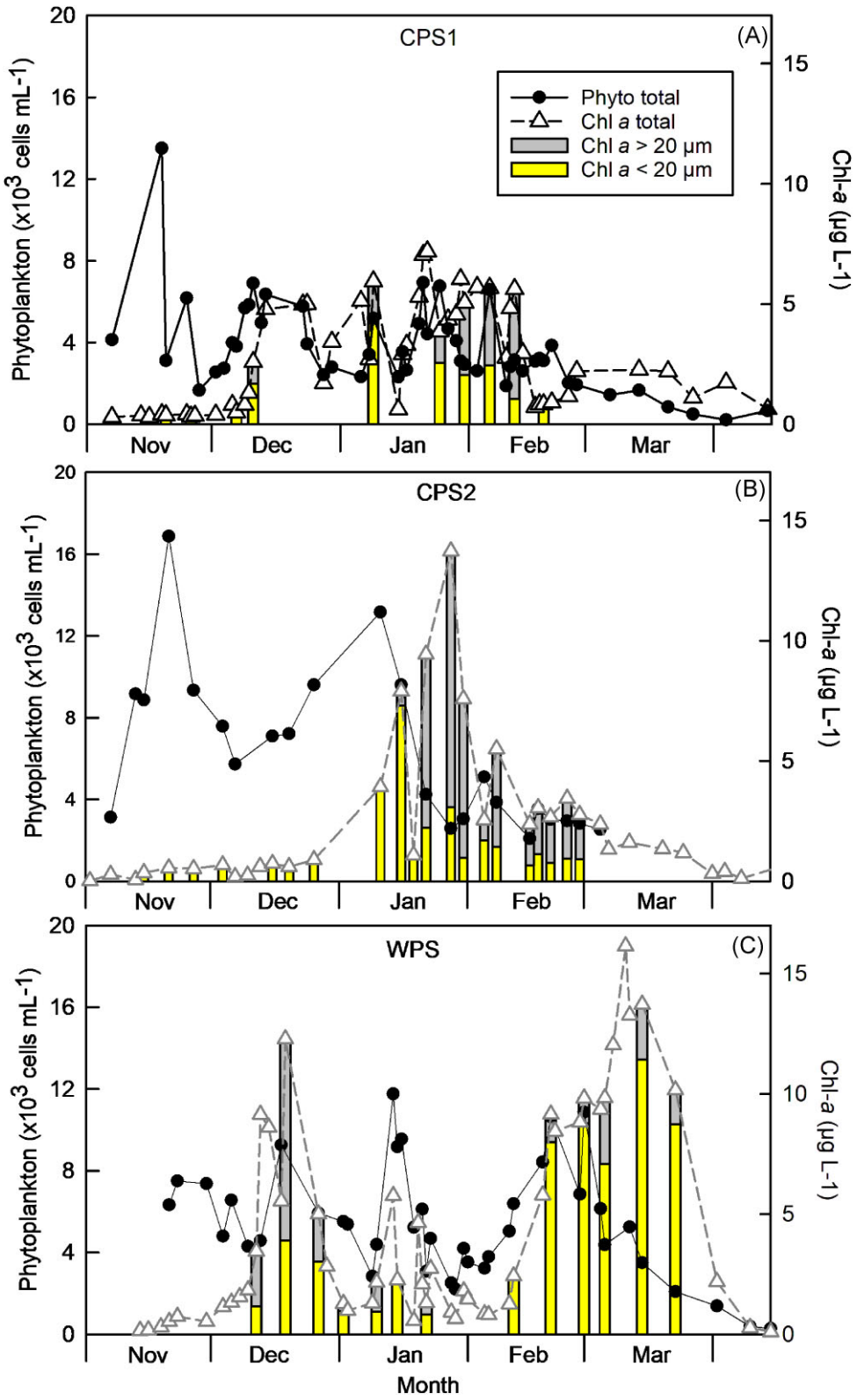

Figure 4. Temporal dynamics of total phytoplankton abundance (Phyto total), total Chl-*a* concentration (Chl-*a* total), and the size-fractionated Chl-*a* (Chl-*a* >20 µm and Chl-*a* <20 µm) concentrations at the RaTS sample site during (A) CPS1, (B) CPS2, and (C) WPS.

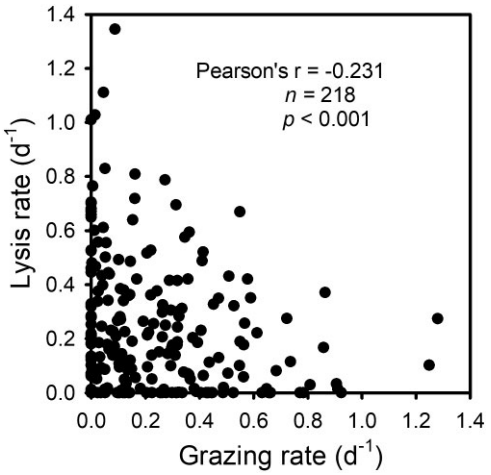

Figure 5. Grazing versus viral lysis rates for all seasons combined.

in standing stock during the cold productive seasons. The equilibrium growth rate, where net growth equals zero (0.41 in CPS1, 0.33 in CPS2, and 0.60 in WPS), is represented by the intercept of the 1:1 and linear regression line. When examining the trend in the dataset (i.e. the linear regression line), positive net growth (or accumulation) occurs to the right of the intercept (along the x-axis) and standing stock decline to the left. During accumulation, the average viral lysis rate was greater than grazing for all three seasons, with a greater difference during the colder seasons of CPS1 (0.27 versus 0.17 d^{-1} respectively, $n = 24$; $P = .029$) and CPS2 (0.26 versus 0.21 d^{-1}, $n = 28$) compared to WPS (0.39 versus 0.37 d^{-1}, $n = 48$). In contrast, during the decline phase (net growth < zero) the share of viral lysis to grazing was similar (i.e. CPS1: 0.18 versus 0.17 d^{-1}, $n = 37$; CPS2: 0.12 versus 0.12 d^{-1}, $n = 31$; and WPS: 0.16 versus 0.18 d^{-1} $n = 50$, respectively; Table 1). More specifically, viral lysis rates were significantly different between accumulation and decline phases in all seasons (i.e. CPS1, 0.27 versus 0.17 d^{-1} $P = .029$; CPS2, 0.26 versus 0.12 d^{-1} $P = .001$; WPS, 0.33 versus 0.16 d^{-1} $P = .002$), but grazing rates were not (i.e. in CPS1, 0.17 versus 0.18 d^{-1} $P = .766$; CPS2, 0.21 versus 0.11 d^{-1} $P = .103$; and WPS, 0.26 versus 0.18 d^{-1} $P = .128$).

Phytoplankton cells and carbon lysed during warm and cold seasons

When comparing the number of cells lost due to lysis and grazing within each of the seasons, CPS1 and CPS2 show similar results as for the specific rate comparison, with more cells lysed during the colder productive seasons of CPS1 and CPS2 (average of 176 ml^{-1} d^{-1} and 256 ml^{-1} d^{-1}, $n = 61$ and 59, respectively) than cells grazed (118 ml^{-1} d^{-1} and 131 ml^{-1} d^{-1}, $n = 61$ and 59, respectively). During the relatively warmer productive season of WPS, the number of cells lysed and grazed were relatively comparable (204 ml^{-1} d^{-1} versus 236 ml^{-1} d^{-1} respectively, $n = 98$). When intercomparing the three, cells produced for CPS1 were significantly lower than for WPS (293 versus 486 ml^{-1} d^{-1}, $P = .006$), as were cells grazed (118 versus 236 cells ml^{-1} d^{-1}, $P < .001$). As for CPS2, only the number of cells grazed was significantly lower (produced 477 and grazed 131 cells ml^{-1} d^{-1}; $P = .043$ for grazed cells). The number of cells lysed was not significantly different between seasons (CPS1, CPS2, and WPS = 176 cells ml^{-1} d^{-1}, 256 cells ml^{-1} d^{-1}, and 204 cells ml^{-1} d^{-1} respectively; Table 1). With all three seasons combined, overall cells lost to viral lysis and grazing were equally important (210 cells ml^{-1} d^{-1} and 175 cells ml^{-1} d^{-1} respectively), as was also found for carbon (3.3 and 2.7 μg C l^{-1} d^{-1}). Although average viral lysis rates and number of cells lysed were higher than grazing during CPS1 and CPS2, but more similar in WPS, average carbon grazed during CPS2 was higher than carbon lysed, and carbon lysed was greater than carbon grazed in WPS and CPS1 (Table 1). This difference was driven mainly by a single large carbon grazing event during CPS2 (Phyto 14 on 22 January 2019, 27% of total carbon grazed; Table S8) and a single large lysis event during WPS (Phyto 14 on 5 March 2013, 33% of total carbon lysed; Table S9). However, when the data from all three seasons were split into warm and cold days (>0°C and <0°C respectively; Tables S1–S3 and Fig. 8), a temperature effect on the proportion of carbon lost due to viral lysis and grazing was again observed. On warm days phytoplankton carbon lysed and grazed were quite similar (averaging 3.20 μg C l^{-1} and 2.91 μg C l^{-1}, respectively), even though carbon grazed was significantly higher based on the median (nonparametric Mann–Whitney rank-sum test, median grazing = 0.74 μg C l^{-1}, lysis = 0.22 μg C l^{-1}, $P = .012$; Fig. 8A and B). This differs from cold days when carbon lost to viruses was significantly higher than carbon lost to grazers (average of 3.42 μg C l^{-1} and 2.45 μg C l^{-1} and median 0.26 μg C l^{-1} and 0.19 μg C l^{-1}, respectively, $P = .031$). When expressed as a percentage, during warm days losses due to viruses were significantly lower with an average of 41% ($P < .001$), unlike cold days where viral infections were significantly higher ($P < .001$) and accounted for 60% of total carbon lost (Fig. 8C and D).

To model phytoplankton carbon flow, the average rates from the accumulation and decline phases (as determined by the linear regression line in Fig. 7), as well as minimum and maximum phytoplankton biomass actually measured (20.5 μg C l^{-1}, 20.6 μg C l^{-1}, and 20.3 μg C l^{-1}; 737 μg C l^{-1}, 885 μg C l^{-1}, and 527 μg C l^{-1} in CPS1, CPS2, and WPS, respectively), were used to model carbon standing stock dynamics (Fig. S4) in relation to carbon produced and lost due to viral lysis and grazing (Fig. 9). The model shows that during the accumulation phase of CPS1 and CPS2, 1.6- and 1.3-fold more carbon was lost to viral lysis (1248 μg C l^{-1} and 1942 μg C l^{-1}, respectively) compared to grazing (773 μg C l^{-1} and 1551 μg C l^{-1}, respectively; Fig. 9A and B). In WPS, however, carbon lost to viral lysis and grazing was comparable (1781 μg C l^{-1} and 1679 μg C l^{-1}, respectively; Fig. 9C). During the decline phase, carbon lost to viruses and grazers was similar in CPS1 (733 μg C l^{-1} and 800 μg C l^{-1}, respectively) and CPS2 (1021 μg C l^{-1} and 1006 μg C l^{-1}, respectively) with more carbon lost to grazers in WPS (1046 μg C l^{-1} and 1431 μg C l^{-1} respectively; Fig. 9C). Similar dynamics were obtained when using average cells (produced and lost) based on the actual rates (Table 1).

Whilst three phytoplankton groups dominated carbon standing stock for all three seasons (i.e. Phyto 8, 14, and 17; 4.5 μm, 12 μm, and 20 μm diameter, respectively), Phyto 14 contributed most to carbon produced and lost in all seasons (CPS1: 69% and 41%; CPS2: 29% and 35%; and WPS: 56% and 64% of total, respectively). During peak abundance of Phyto 14 in late December of CPS1, viral lysis was responsible for the majority of carbon lost (92% or 77 μg C l^{-1} d^{-1}; Table S7), as also found during large lysis events of Phyto 14 throughout WPS (Biggs et al. 2021; Table S9). Similarly, Phyto 14 contributed most to total carbon lysed (42%) during the largest lysis event of CPS2 (72 μg C l^{-1} d^{-1}; on 22 January; Table S8). However, a significantly lower total standing stock of Phyto 14 was observed during CPS1 and CPS2 ($n_1 = 40$ and 23, $n_2 = 50$ and 40, $P = .001$ and $< .001$, respectively), coinciding with lower average Chl-*a* concentrations (2.7 μg l^{-1} and 2.4 μg l^{-1}, respectively) when compared to WPS (4.3 μg l^{-1}; Fig. 4). Differences in the size class of carbon standing stock (at the start of the

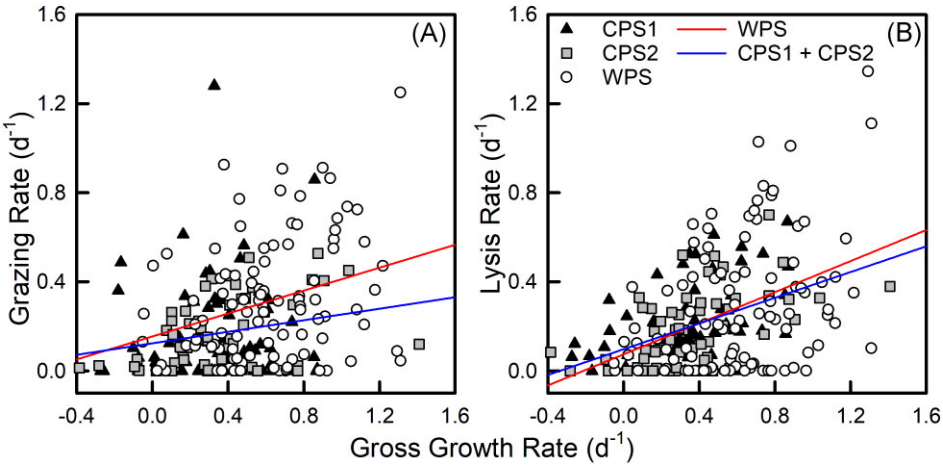

Figure 6. Gross growth rates versus (A) grazing and (B) viral lysis. Linear regressions are shown for CPS1 and CPS2 combined (CPS1 + CPS2) as well as WPS.

Table 1. Average rates, cells, and carbon produced (growth) and lost due to viral lysis (Ly) and grazing (Gr), in accumulation and decline phases during CPS1, CPS2, and WPS as well as all seasons combined (ALL). Average values are based on the data that forms the linear regression line either to the right (accumulation) or left (decline) of the intercept identified in Fig. 8.

		Season average			Accumulation			Decline		
	Season	Growth	Ly	Gr	Growth	Ly	Gr	Growth	Ly	Gr
Rates (d^{-1})	CPS1	0.35	0.21	0.18	0.61	0.27	0.17	0.19	0.17	0.18
	CPS2	0.35	0.18	0.16	0.59	0.26	0.21	0.13	0.12	0.11
	WPS	0.61	0.29	0.31	0.87	0.39	0.37	0.36	0.19	0.26
	ALL	0.47	0.24	0.23	0.75	0.33	0.26	0.26	0.16	0.18
Cells (ml^{-1} d^{-1})	CPS1	293	176	118	464	237	139	182	136	104
	CPS2	477	256	131	784	411	129	200	117	133
	WPS	486	204	236	611	218	243	366	189	229
	ALL	429	210	174	602	273	210	283	157	145
Carbon (μg l^{-1} d^{-1})	CPS1	6.10	2.49	1.43	13.2	4.6	1.0	1.5	1.1	1.7
	CPS2	8.21	2.97	3.11	14.2	4.9	4.4	2.8	1.2	2.0
	WPS	7.42	4.03	3.18	9.7	3.3	4.1	5.2	4.7	2.3
	ALL	7.26	3.31	2.67	11.2	4.5	3.3	3.9	2.1	2.4

experiments) were also observed between seasons, with greater contributions by the larger-sized diatoms Phyto 15–17 in the colder CPS1 (48%) and CPS2 (48%), whilst in WPS the second largest carbon contributor (after a 69% contribution by Phyto 14) was the high temperature associated smaller-sized diatom Phyto 8 (14%; Biggs et al. 2019). Even though differences in the size class of carbon were observed between the colder and warmer seasons, when total carbon produced was plotted against total carbon lost for all seasons combined, a highly significant relationship was observed with the slope of the linear regression line close to the 1:1 line (Fig. 10).

Discussion

Method considerations in natural waters

Although marine viruses are the most abundant biological entities in the ocean, and rising evidence suggests that viruses are a significant cause of phytoplankton mortality, measuring the impact of viruses remains challenging. Despite it's limitations (Evans et al. 2003, Baudoux et al. 2006, 2007, Kimmance et al. 2007, Kimmance and Brussaard 2010), the modified dilution method still remains the only method of directly and simultaneously measuring rates of viral lysis and microzooplankton grazing of phytoplankton.

When using this method, mesozooplankton (>200 µm) grazing rates are not determined. Large zooplankton (such as krill) are inefficient grazers on pico- and nano-sized phytoplankton (<20 µm; Haberman et al. 2003, Conroy et al. 2024). Grazing by mesozooplankton is also likely to influence phytoplankton dynamics, as suggested by our previous study conducted throughout WPS and CPS1 (Biggs et al. 2020), where low phytoplankton biomass (specifically the decline of the diatom dominated spring bloom in CPS1 and WPS) coincided with the seasonal peak in mesozooplankton abundance (and low light due to high phytoplankton biomass). Although diatoms are an important prey of krill, so are copepods and microzooplankton (Conroy et al. 2024). Predation on microzooplankton would serve to reduce microzooplankton grazing on phytoplankton. As mesozooplankton were removed from the dilution incubations, there is the potential that microzooplankton grazing may at times have even been overestimated in our experiments. Furthermore, the assay is based on loss of phytoplankton cells and as such viral infection needs to result in cell lysis of the host to be included. As not all phytoplankton viruses lyse their host within 24 h (particularly diatom viruses seem to take

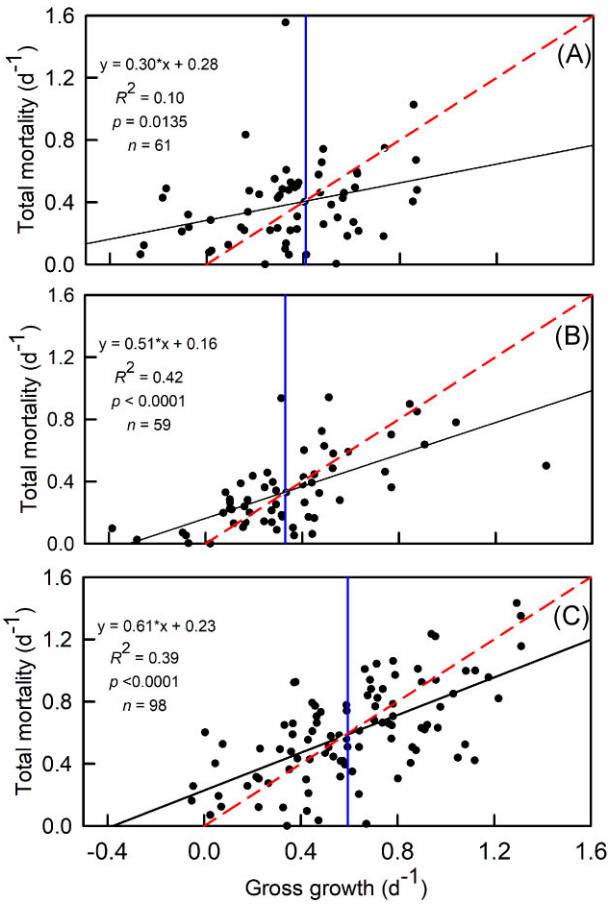

Figure 7. Phytoplankton (Phyto 1–17) gross growth versus total mortality rates for (A) CPS1, (B) CPS2, and (C) WPS. The 1:1 line (red dashed) and linear regression line (solid black) are presented in each subplot, as well as the intercept (blue line).

longer; see Supplement Table S1 in Edwards and Steward 2018), we may even underestimate viral lysis rates. Micro-sized phytoplankton (20–200 µm) are generally too low in abundance to allow the dilution-based approach. The lack of *in situ* viral lysis rates of this size class of phytoplankton hinders a direct comparison with mesozooplankton grazing rates. Still, the <20-µm phytoplankton size fraction investigated in the current study comprised 67% of total Chl-*a* in CPS1, 57% in CPS2, and 70% in WPS, illustrating the importance of the smaller phytoplankton for ecosystem functioning.

Temperature-related interannual differences

In Antarctic coastal and shelf sea regions such as Ryder Bay, temperature and light availability are generally the primary drivers of phytoplankton growth rates during the summer (Arrigo et al. 2015, Rozema et al. 2017a, Biggs et al. 2019, Joy-Warren et al. 2019). Temperature imposes a fundamental control on metabolic processes (Boscolo-Galazzo et al. 2018) and during CPS1 and CPS2 the maximum potential growth of phytoplankton may have been reduced as relatively low average temperatures during the sampling periods (−0.37°C and −0.42°C, respectively) coincided with significantly lower rates of phytoplankton gross growth (0.35 and 0.35 d^{-1}) compared to the warmer WPS (0.37°C and 0.61 d^{-1}). It is improbable that light was a major driver of the differences in phytoplankton growth, as average irradiance in CPS2 was 3-fold higher than in WPS (and 2-fold higher than CPS1).

Unlike rates of viral lysis, grazing rates were also significantly lower during the colder productive seasons, suggesting a greater reduction in rates of grazing (compared to viral lysis) when temperatures are reduced. As microzooplankton are generally larger than their phytoplankton prey, due to the size scaling of metabolic rates (Finkel et al. 2004) low temperature seasons may result in a larger reduction in grazer growth potential compared to that of phytoplankton (Rose and Caron 2007, Rose et al. 2013). Moreover, prey abundance is a key factor controlling microzooplankton growth and so their grazing impact can be expected to be relatively low in the early stages of bloom development (especially after mid-winter) when phytoplankton prey availability and temperatures are relatively low (Sherr and Sherr 2009). These could result in a relative overabundance (net growth) of algal cells when temperatures are low. As such, relatively higher contact rates may be maintained between virus and host, resulting in viral lysis being the predominant loss factor regulating increases in standing stock during colder seasons. This exemplifies a competition effect, where the balance between numbers of phytoplankton (host) and infective viruses would likely result in a threshold contact rate above which large population declines are observed (Bratbak et al. 1993, Singh et al. 2004, Brussaard et al. 2005a) and could explain the trend that high viral lysis was often observed alongside low grazing, and *vice versa*. Additionally, lower grazing may mean a higher proportion of successful viral infections, especially in the case that grazing preferentially targets infected cells (Evans and Wilson 2008). These effects could explain why viral lysis has increased importance in colder productive seasons.

Even though average rates of viral lysis were not significantly different between seasons, the rates in the cold seasons were slightly lower compared to WPS (0.21 and 0.18 d^{-1} compared to 0.29 d^{-1}) and temperature may have been restrictive to some extent (Demory et al. 2017, Maat et al. 2017, Piedade et al. 2018). The optimal temperature for lytic replication (i.e. the temperature that generates fast host lysis and/or high viral yield) generally matches the host optimal growth temperature and the impact of temperature on viral infection could arise from changes in host metabolism (Demory et al. 2017). At the same time, phytoplankton-specific thermal thresholds and temperature growth optima (Boyd et al. 2013, Coello-Camba and Agustí 2017, Wang and Smith 2021) are expected to result in a diverse response to the same change in temperature (e.g. temperatures >0°C and <0°C). For example, Phyto 1 abundances were mainly associated with higher light availability rather than temperature (CPS1 and WPS; Biggs et al. 2019), and no significant differences between the seasons for growth or losses were found for Phyto 1 (Fig. S5A). In contrast, the nano-sized cryptophytes Phyto 6 were associated with high temperature in WPS (Biggs et al. 2019), agreeing with lower abundances and reduced rates of gross growth and viral lysis in CPS1 and CPS2 (Fig. S5B). If temperature is a major driver of cryptophyte growth and viral lysis rates, future changes in cryptophyte importance should not only be derived from standing stock data but also include activity measurements (production and loss rates). Antarctic cryptophytes have previously been associated with reduced salinities (Buma et al. 1992, Moline et al. 1997, 2004, Mendes et al. 2013) but more recent research indicates temperature could indeed be a primary driver in the WAP region (Mendes et al. 2017, Biggs et al. 2019, Hamilton et al. 2021).

The smaller-sized diatoms Phyto 8 (4.5 µm diameter) were also associated with higher temperature in WPS (Biggs et al. 2019), where they were the second largest contributor to total carbon standing stock (14% during the experiments and 20% overall). A greater growth potential of Phyto 8 during WPS (Fig. S5C) may have

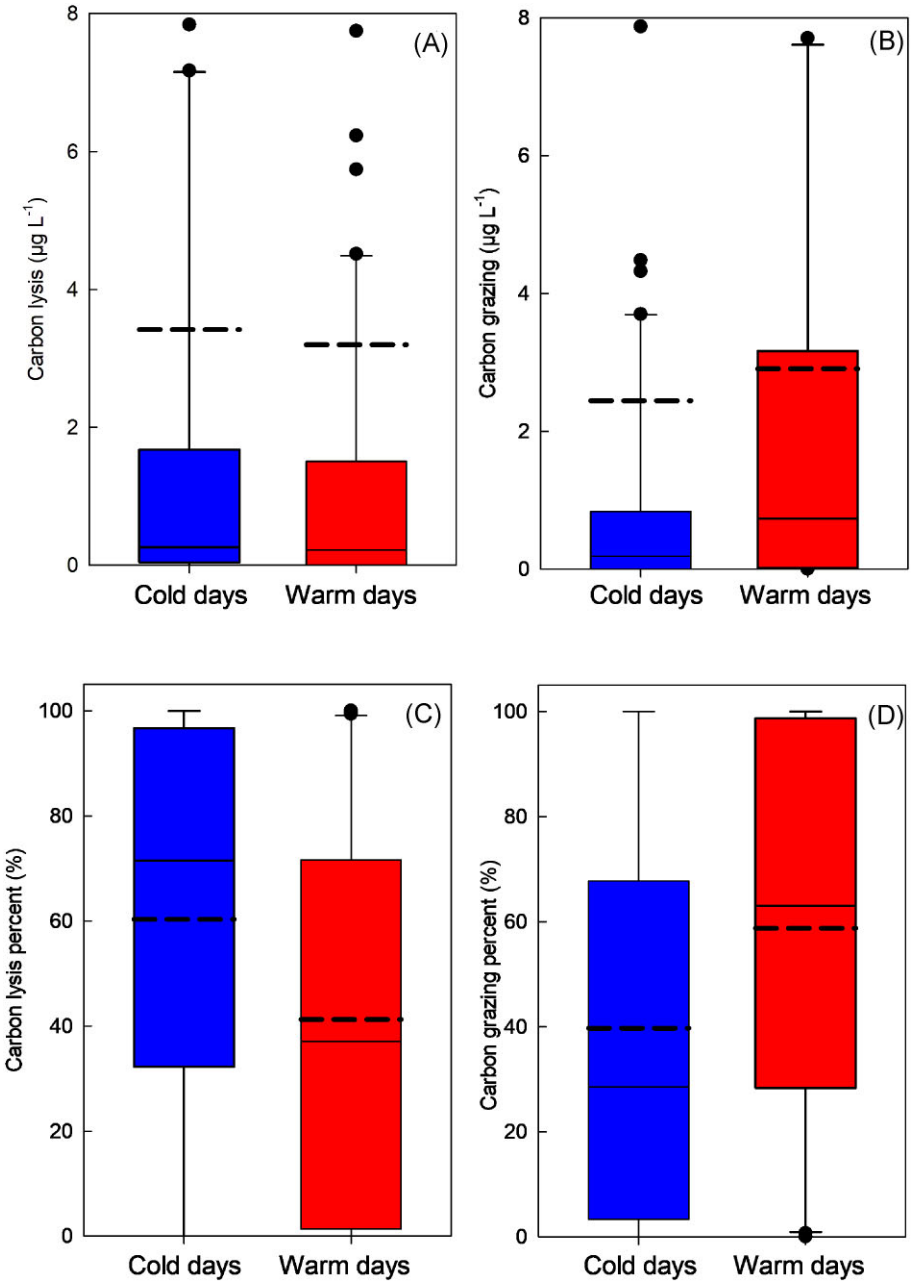

Figure 8. Carbon lost on cold and warm days due to viral lysis and grazing. Absolute carbon concentrations lost to viral lysis (A) and grazing (B) as well as the % of carbon lost due to viral lysis (C) and grazing (D), during CPS1, CP2, and WPS combined. Days on which the dilution experiments were performed were considered cold if temperature at a depth of 15 m was <0°C and warm if >0°C. The boundary of the box closest to zero indicates the 25th percentile, the solid line within the box marks the median, the dashed line marks the mean, and the boundary of the box farthest from zero indicates the 75th percentile. Whiskers (error bars) above and below the box indicate the 90th and 10th percentiles. Note: box plot *y*-axis in subplot (A) and (C) was cut to better visualize boxes. Maximum values were 131 µg C l^{-1} for lysis on warm days in (A) and 77 µg C l^{-1} for grazing on cold days in (B).

provided a competitive advantage, compared to CPS1 and CPS2, where lower temperatures and prolonged sea ice melt coincided with higher abundances of the larger-sized Phyto 17 (Table S2 and Fig. S3B; Biggs et al. 2019). Although numbers of Phyto 17 were relatively low overall (mean = 72 ml^{-1} in CPS1 and 58 ml^{-1} in CPS2), its larger cell size (20 µm diameter) resulted in a 48% and 28% (respectively) contribution to total carbon standing stock during the experiments. We speculate that with increasing temperature by global warming, the share of Phyto 17 will quickly reduce in favour of the smaller diatoms Phyto 8 and cryptophytes Phyto 6 (4–5 µm diameter), negatively impacting copepod production, and thus transfer of matter and energy to higher trophic levels (Irigoien et al. 2014, Dezutter et al. 2019, Biggs et al. 2020).

Viral lysis and grazing in relation to gross growth

For all seasons the greater variation in rates of viral lysis (compared to grazing) between accumulation and decline phases suggests that, irrespective of temperature, rates of viral lysis are more tightly coupled to phytoplankton growth than rates of grazing. We observed a significant positive relationship between viral lysis and gross growth rates for many phytoplankton groups such as *Phaeocystis* Phyto 3, cryptophytes Phyto 6, and diatoms Phyto 8, 9, and 14

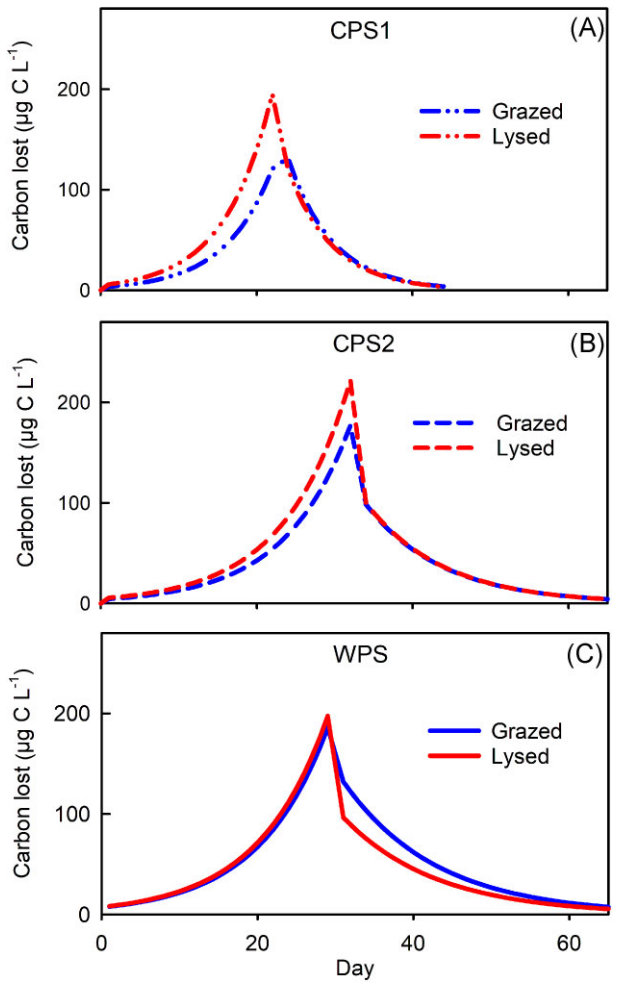

Figure 9. Modelled phytoplankton carbon lost due to grazing and viral lysis (µg carbon l^{-1}) using seasonal average rates (of grazing and viral lysis) from accumulation and decline phases identified in Fig. 8, during (A) CPS1, (B) CPS2, and (C) WPS.

as well as Phyto 15–17 combined. Positive relationships between host gross growth rate and viral lysis have been demonstrated for bacteria and phytoplankton both in the laboratory and field (e.g. Bratbak et al. 1998, Middelboe 2000, Baudoux et al. 2007, Gann et al. 2020). This positive coupling between host growth and viral lysis is expected due to the reliance of viral proliferation on host cell metabolism. Higher growth rates are supported by increased rates of ribosome biogenesis, which are also essential for the synthesis of viral proteins. This codependence on host cellular machinery for both viral replication and host physiology is likely stricter for viral production and subsequent host cell lysis than for grazing. We did observe a significant positive relationship between phytoplankton growth and grazing (Fig. 6A), in line with previous studies (Pearce et al. 2008, Landry et al. 2009, 2011), but this was limited to only Phyto 1, 4, and 8. Grazers can be selective in their prey choices, primarily driven by prey size (Kiørboe 2011, Litchman et al. 2021), whereas viral infection are generally considered to be more host species-specific. A stricter coupling between viral lysis rates and phytoplankton gross growth (than grazing) would become exemplified during periods of high phytoplankton growth in low temperature seasons as viruses are quicker to respond to increased rates of phytoplankton growth.

Cell size and carbon losses

The model results indicate notable variations in the fate of carbon during phytoplankton accumulation phases in the cold productive seasons (CPS1 and CPS2), compared to the warmer season (WPS). Specifically, during CPS1 and CPS2, a larger proportion of carbon was lost to viral lysis than to grazing, with ratios of 1.6-fold and 1.3-fold, respectively. In contrast, during phytoplankton accumulation in the warmer WPS, losses due to viral lysis and grazing were more balanced, with a ratio of 1:1. Furthermore, higher concentrations of carbon were lost during WPS overall, with an average of 30 µg C l^{-1} d^{-1} and 17 µg C l^{-1} d^{-1} for the larger- (>10 µm) and smaller (<10 µm)-sized phytoplankton groups (respectively), compared to 14 µg C l^{-1} d^{-1} and 8 µg C l^{-1} d^{-1} (respectively) during CPS1 and CPS2 (Fig. 11). This indicates greater food web carbon and energy flux, both through the viral shunt (stimulating the microbial loop) and to higher trophic levels by grazing (stimulating microzooplankton communities, Fig. 11).

However, it is important to note that the model does not account for temporal differences in phytoplankton size class or taxonomy between warm and cold seasons. Phyto 14, characterized by an average 12 µm cell diameter, significantly contributed to overall seasonal carbon flow in all seasons, representing 51% of production and 53% of losses. This is important as diatoms within this size class allow larger zooplankton (such as copepods and krill) direct access to primary production and hence efficient transfer of energy and matter from phytoplankton to large grazers. Although we did not assess mesozooplankton grazing rates, high biomass lysis events on Phyto 14, such as that occurring in March of WPS, may exert a disproportionately significant influence on energy and carbon transfer, as not only does the viral shunt stimulate microbial utilization (Fig. S6) and community respiration, but this high biomass lysis event coincided with both the seasonal peak in Chl-*a* concentrations as well as the annual peak of key primary consumers (*Calanoides acutus*; Biggs et al. 2020). Thus, although rates of viral lysis and grazing were more balanced during WPS, higher contributions from smaller-sized cryptophytes and diatoms were observed, coupled with relatively intense lysis of the larger diatom Phyto 14 that diverted an average of 19 µg C l^{-1} d^{-1} towards the dissolved organic carbon pool (see Fig. 11; carbon viral lysis >10 µm). This likely resulted in a substantial reduction of carbon transfer to higher trophic levels (copepods and krill). Further comprehensive seasonal investigations into the types of phytoplankton viruses present in Antarctic waters are crucial for gaining a better understanding of viral control over phytoplankton diversity and production in an ocean characterized by global connectivity.

Conclusions

Our results suggest a synergistic relationship between rates of gross growth and temperature that combine to result in a greater share of viral lysis when temperatures are low, particularly pronounced during periods of phytoplankton accumulation. Furthermore, lower rates of gross growth and total mortality indicate reduced trophic transfer of carbon and energy from primary producers to microzooplankton during cold productive seasons (average temperature <0°C).

Although carbon flows were higher during the WPS, as indicated by increased rates of gross growth and total mortality, greater contributions by smaller-sized cells, combined with high biomass lysis events of an important biomass producer (both in terms of cell size and taxonomy), may have resulted in a substan-

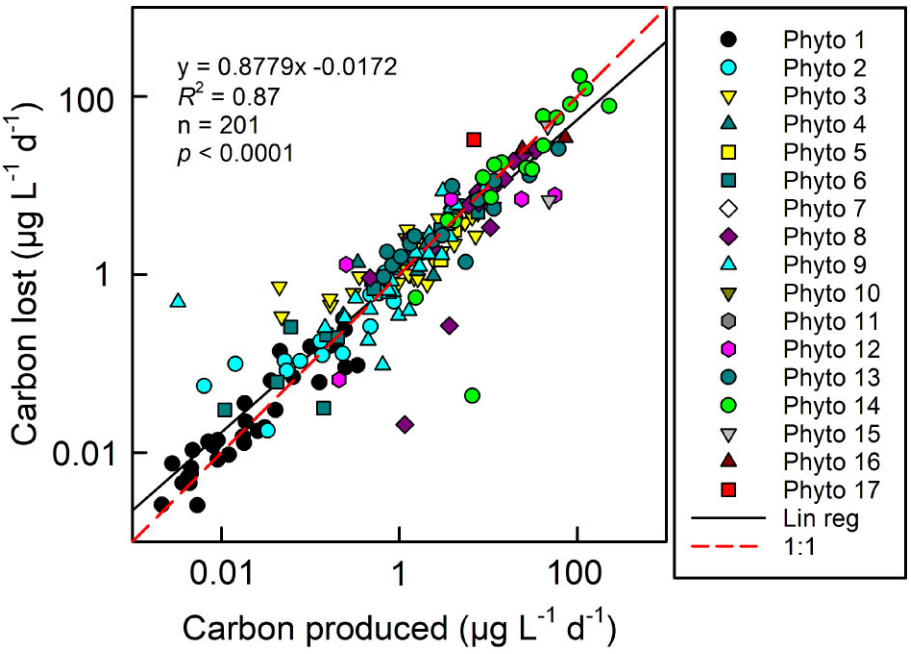

Figure 10. Phytoplankton carbon lost (i.e. lysis plus grazing,) plotted against carbon produced for all seasons (i.e. CPS1, CPS2, and WPS), obtained after conversion of the different phytoplankton group abundances [integrated over time using the specific viral lysis, grazing, total mortality, and gross growth rates (d^{-1})]. The 1:1 and linear regression lines are included. Note: zeros and negative values were excluded from log transformed carbon data, $n = 3$ and 14, respectively.

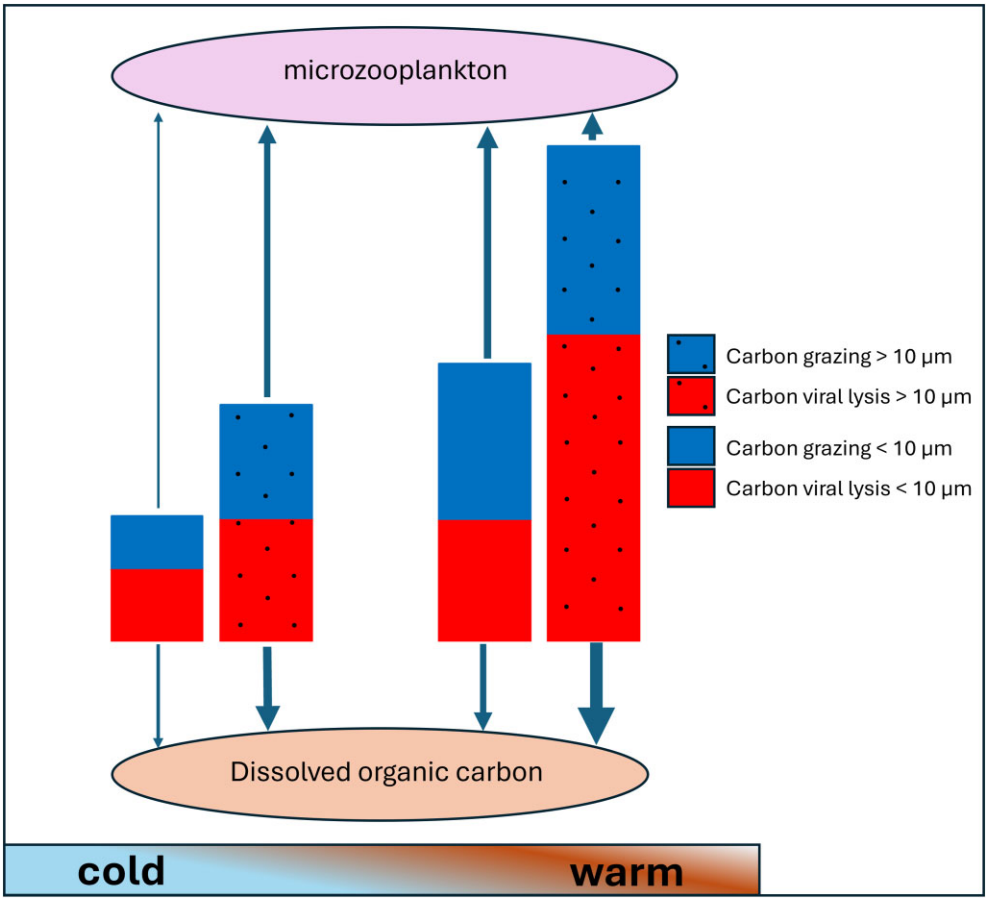

Figure 11. Average phytoplankton carbon lost due to viral lysis and grazing for both larger- (>10 µm, Phyto 14–17) and smaller (>10 µm, Phyto 1–13)-sized phytoplankton groups. Averages were calculated based on the sum of carbon per loss factor and per size fraction for each experiment in warm (WPS, $n = 15$) and cold (CPS1 + CPS2, $n = 27$) seasons.

tial reduction in the efficiency of carbon and energy transfer from primary producers to larger-sized grazers such as copepods and krill.

This study reaffirms that viral lysis is an importance loss factor for Antarctic phytoplankton and suggests a tighter coupling of viral lysis rates with phytoplankton growth compared to grazing. It is essential to include viral lysis in monitoring efforts to allow for an improved insight on the role of temperature for the relative importance of viral lysis compared to grazing. More baseline rate data is critically needed for a better understanding of viral lysis and its subsequent impact on trophic transfer efficiency and biogeochemical cycling.

Acknowledgements

We thank the British Antarctic Survey for their logistical support and cooperation during the field campaign as well as Dorien Verheyen, Nisma Abdelmalik, and Monika Krolikowski for field assistance.

Author contributions

Tristan E.G. Biggs (Data curation, Formal analysis, Investigation, Methodology, Visualization, Writing – original draft, Writing – review & editing), Gonçalo J. Piedade (Formal analysis, Investigation, Methodology, Visualization, Writing – original draft, Writing – review & editing), Ella M. Wesdorp (Formal analysis, Investigation, Writing – review & editing), Michael P. Meredith (Conceptualization, Methodology, Supervision, Writing – review & editing), Claire Evans (Funding acquisition, Project administration, Resources, Writing – review & editing), and Corina P.D. Brussaard (Conceptualization, Funding acquisition, Investigation, Project administration, Resources, Supervision, Visualization, Writing – original draft, Writing – review & editing)

Supplementary data

Supplementary data is available at *FEMSEC Journal* online.

Conflict of interest: The authors declare no competing interests.

Funding

This work was part of the POMVIDDY project (grant ALWPP.2016.019 awarded to C.P.D.B.), which was supported by the Dutch Research Council (NWO), within the Netherlands Polar Programme. C.E. was supported by Natural Environment Research Council (NERC) Independent Research Fellowship NE/M018806/1. M.M. was supported by NERC award NE/W004933/1 (BIOPOLE).

References

Agirbas E, Feyzioglu AM, Kopuz U *et al.* Phytoplankton community composition in the south-eastern Black Sea determined with pigments measured by HPLC-CHEMTAX analyses and microscopy cell counts. *J Mar Biol Assoc UK* 2015;**95**:35–52. https://doi.org/10.1017/S0025315414001040.

Arrigo KR, van Dijken GL, Strong AL. Environmental controls of marine productivity hot spots around Antarctica. *J Geophys Res Ocean* 2015;**120**:5545–65. https://doi.org/10.1002/2015JC010888.

Baudoux A-C, Noordeloos AAM, Veldhuis MJW *et al.* Virally induced mortality of *Phaeocystis globosa* during two spring blooms in temperate coastal waters. *Aquat Microb Ecol* 2006;**44**:207–17. https://doi.org/10.3354/ame044207.

Baudoux A-C, Veldhuis MJW, Witte HJ *et al.* Viruses as mortality agents of picophytoplankton in the deep chlorophyll maximum layer during IRONAGES III. *Limnol Oceanogr* 2007;**52**:2519–29. https://doi.org/10.4319/lo.2007.52.6.2519.

Biggs TEG, Alvarez-Fernandez S, Evans C *et al.* Antarctic phytoplankton community composition and size structure: importance of ice type and temperature as regulatory factors. *Polar Biol* 2019;**42**:1997–2015. https://doi.org/10.1007/s00300-019-02576-3.

Biggs TEG, Brussaard CPD, Evans C *et al.* Plasticity in dormancy behaviour of *Calanoides acutus* in Antarctic coastal waters. *ICES J Mar Sci* 2020;**77**:1738–51. https://doi.org/10.1093/icesjms/fsaa042.

Biggs TEG, Huisman J, Brussaard CPD. Viral lysis modifies seasonal phytoplankton dynamics and carbon flow in the Southern Ocean. *ISME J* 2021;**15**:3615–22. https://doi.org/10.1038/s41396-021-01033-6.

Biggs TEG, Rozema PD, Evans C *et al.* Control of Antarctic phytoplankton community composition and standing stock by light availability. *Polar Biol* 2022;**45**:1635–53. https://doi.org/10.1007/s00300-022-03094-5.

Boscolo-Galazzo F, Crichton KA, Barker S *et al.* Temperature dependency of metabolic rates in the upper ocean: a positive feedback to global climate change?. *Glob Planet Change* 2018;**170**:201–12. https://doi.org/10.1016/j.gloplacha.2018.08.017.

Boyd PW, Rynearson TA, Armstrong EA *et al.* Marine phytoplankton temperature versus growth responses from polar to tropical waters—outcome of a scientific community-wide study. *PLoS One* 2013;**8**:e63091. https://doi.org/10.1371/journal.pone.0063091.

Bratbak G, Egge JK, Heldal M. Viral mortality of the marine alga *Emiliania huxleyi* (Haptophyceae) and termination of algal blooms. *Mar Ecol Prog Ser* 1993;**93**:39–48. https://doi.org/10.3354/meps093039.

Bratbak G, Jacobsen A, Heldal M *et al.* Virus production in *Phaeocystis pouchetii* and its relation to host cell growth and nutrition. *Aquat Microb Ecol* 1998;**16**:1–9. https://doi.org/10.3354/ame016001.

Brussaard CPD, Kuipers B, Veldhuis MJW. A mesocosm study of *Phaeocystis globosa* population dynamics I. Regulatory role of viruses in bloom control. *Harmful Algae* 2005a;**4**:859–74. https://doi.org/10.1016/j.hal.2004.12.015.

Brussaard CPD, Mari X, van Bleijswijk JDL *et al.* A mesocosm study of *Phaeocystis globosa* (Prymnesiophyceae) population dynamics II. Significance for the microbial community. *Harmful Algae* 2005b;**4**:875–93. https://doi.org/10.1016/j.hal.2004.12.012.

Brussaard CPD, Martínez J. Algal bloom viruses. *Plant Virus* 2008;**2**:1–13.

Brussaard CPD, Peperzak L, Beggah S *et al.* Immediate ecotoxicological effects of short-lived oil spills on marine biota. *Nat Commun* 2016;**7**:1–11. https://doi.org/10.1038/ncomms11206.

Brussaard CPD, Wilhelm SW, Thingstad F *et al.* Global-scale processes with a nanoscale drive: the role of marine viruses. *ISME J* 2008;**2**:575–8. https://doi.org/10.1038/ismej.2008.31.

Buma AGJ, Gieskes WWC, Thomsen HA. Abundance of cryptophyceae and chlorophyll *b*-containing organisms in the Weddell–Scotia Confluence area in the spring of 1988. *Polar Biol* 1992;**12**:43–52. https://doi.org/10.1007/BF00239964.

Clarke A, Meredith MP, Wallace MI *et al.* Seasonal and interannual variability in temperature, chlorophyll and macronutrients in northern Marguerite Bay, Antarctica. *Deep Res Part II Top Stud Oceanogr* 2008;**55**:1988–2006. https://doi.org/10.1016/j.dsr2.2008.04.035.

Coello-Camba A, Agustí S. Thermal thresholds of phytoplankton growth in polar waters and their consequences for a warming

polar ocean. *Front Mar Sci* 2017;**4**:1–12. https://doi.org/10.3389/fmars.2017.00168.

Conroy JA, Steinberg DK, Nardelli SC *et al.* Omnivorous summer feeding by juvenile Antarctic krill in coastal waters. *Limnol Oceanogr* 2024;**69**:874–87. https://doi.org/10.1002/lno.12533.

Demory D, Arsenieff L, Simon N *et al.* Temperature is a key factor in *Micromonas* – virus interactions. *ISME J* 2017;**11**:601–12. https://doi.org/10.1038/ismej.2016.160.

DeVries T, Primeau F, Deutsch C. The sequestration efficiency of the biological pump. *Geophys Res Lett* 2012;**39**:L13601. https://doi.org/10.1029/2012GL051963.

Dezutter T, Lalande C, Dufresne C *et al.* Mismatch between microalgae and herbivorous copepods due to the record sea ice minimum extent of 2012 and the late sea ice break-up of 2013 in the Beaufort Sea. *Prog Oceanogr* 2019;**173**:66–77. https://doi.org/10.1016/j.pocean.2019.02.008.

Edwards KF, Steward GF. Host traits drive viral life histories across phytoplankton viruses. *Am Nat* 2018;**191**:566–81. https://doi.org/10.1086/696849.

Edwards KF, Thomas MK, Klausmeier CA *et al.* Phytoplankton growth and the interaction of light and temperature: a synthesis at the species and community level. *Limnol Oceanogr* 2016;**61**:1232–44. https://doi.org/10.1002/lno.10282.

Eich C, Biggs TEG, van de Poll WH *et al.* Ecological importance of viral lysis as a loss factor of phytoplankton in the Amundsen Sea. *Microorganisms* 2022;**10**:1–20. https://doi.org/10.3390/microorganisms10101967.

Evans C, Archer SD, Jacquet S *et al.* Direct estimates of the contribution of viral lysis and microzooplankton grazing to the decline of a *Micromonas* spp. population. *Aquat Microb Ecol* 2003;**30**:207–19. https://doi.org/10.3354/ame030207.

Evans C, Brandsma J, Pond DW *et al.* Drivers of interannual variability in virioplankton abundance at the coastal Western Antarctic Peninsula and the potential effects of climate change. *Environ Microbiol* 2017;**19**:740–55. https://doi.org/10.1111/1462-2920.13627.

Evans C, Wilson WH. Preferential grazing of *Oxyrrhis marina* on virus infected *Emiliania huxleyi*. *Limnol Oceanogr* 2008;**53**:2035–40. https://doi.org/10.4319/lo.2008.53.5.2035.

Finkel Z, Irwin A, Schofield O. Resource limitation alters the 3/4 size scaling of metabolic rates in phytoplankton. *Mar Ecol Prog Ser* 2004;**273**:269–79. https://doi.org/10.3354/meps273269.

Gann ER, Gainer PJ, Reynolds TB *et al.* Influence of light on the infection of *Aureococcus anophagefferens* CCMP 1984 by a "giant virus". *PLoS One* 2020;**15**:e0226758. https://doi.org/10.1371/journal.pone.0226758.

Garibotti IA, Vernet M, Kozlowski WA *et al.* Composition and biomass of phytoplankton assemblages in coastal Antarctic waters: a comparison of chemotaxonomic and microscopic analyses. *Mar Ecol Prog Ser* 2003;**247**:27–42. https://doi.org/10.3354/meps247027.

Garrison DL, Gowing MM, Hughes MP *et al.* Microbial food web structure in the Arabian Sea: a US JGOFS study. *Deep Sea Res Part II Top Stud Oceanogr* 2000;**47**:1387–422. https://doi.org/10.1016/S0967-0645(99)00148-4.

Haberman KL, Quetin LB, Ross RM. Diet of the Antarctic krill (*Euphausia superba* Dana). *J Exp Mar Bio Ecol* 2003;**283**:79–95. https://doi.org/10.1016/S0022-0981(02)00466-5.

Hamilton M, Mascioni M, Hehenberger E *et al.* Spatiotemporal variations in Antarctic protistan communities highlight phytoplankton diversity and seasonal dominance by a novel cryptophyte lineage. *mBio* 2021;**12**. https://doi.org/10.1128/mBio.02973-21.

Irigoien X, Klevjer TA, Røstad A *et al.* Large mesopelagic fishes biomass and trophic efficiency in the open ocean. *Nat Commun* 2014;**5**:3271. https://doi.org/10.1038/ncomms4271.

Irion S, Christaki U, Berthelot H *et al.* Small phytoplankton contribute greatly to CO_2-fixation after the diatom bloom in the Southern Ocean. *ISME J* 2021;**15**:2509–22. https://doi.org/10.1038/s41396-021-00915-z.

Joy-Warren HL, Dijken GL, Alderkamp A *et al.* Light is the primary driver of early season phytoplankton production along the Western Antarctic Peninsula. *J Geophys Res Ocean* 2019;**124**:7375–99. https://doi.org/10.1029/2019JC015295.

Kauko HM, Hattermann T, Ryan-Keogh T *et al.* Phenology and environmental control of phytoplankton blooms in the Kong Håkon VII Hav in the Southern Ocean. *Front Mar Sci* 2021;**8**:1–24. https://doi.org/10.3389/fmars.2021.623856.

Kimmance SA, Brussaard CPD. Estimation of viral-induced phytoplankton mortality using the modified dilution method. In: Wilhelm SW, Weinbauer MG, Suttle CA (eds), *Manual of Aquatic Viral Ecology*. Waco, TX: American Society of Limnology and Oceanography, 2010, 65–73.

Kimmance SA, Wilson WH, Archer SD. Modified dilution technique to estimate viral versus grazing mortality of phytoplankton: limitations associated with method sensitivity in natural waters. *Aquat Microb Ecol* 2007;**49**:207–22. https://doi.org/10.3354/ame01136.

Kiørboe T. How zooplankton feed: mechanisms, traits and trade-offs. *Biol Rev* 2011;**86**:311–39. https://doi.org/10.1111/j.1469-185X.2010.00148.x.

Krumhardt KM, Long MC, Sylvester ZT *et al.* Climate drivers of Southern Ocean phytoplankton community composition and potential impacts on higher trophic levels. *Front Mar Sci* 2022;**9**:1–18. https://doi.org/10.3389/fmars.2022.916140.

Landry MR, Ohman MD, Goericke R *et al.* Lagrangian studies of phytoplankton growth and grazing relationships in a coastal upwelling ecosystem off Southern California. *Prog Oceanogr* 2009;**83**:208–16. https://doi.org/10.1016/j.pocean.2009.07.026.

Landry MR, Selph KE, Taylor AG *et al.* Phytoplankton growth, grazing and production balances in the HNLC equatorial Pacific. *Deep Sea Res Part II Top Stud Oceanogr* 2011;**58**:524–35. https://doi.org/10.1016/j.dsr2.2010.08.011.

Le Quéré C, Buitenhuis ET, Moriarty R *et al.* Role of zooplankton dynamics for Southern Ocean phytoplankton biomass and global biogeochemical cycles. *Biogeosciences* 2016;**13**:4111–33. https://doi.org/10.5194/bg-13-4111-2016.

Li WKW, Dickie PM. Monitoring phytoplankton, bacterioplankton, and virioplankton in a coastal inlet (Bedford Basin) by flow cytometry. *Cytometry* 2001;**44**:236–46. https://doi.org/10.1002/1097-0320(20010701)44 : 3(236::AID-CYTO1116)3.0.CO;2-5.

Litchman E, Edwards KF, Boyd PW. Toward trait-based food webs: universal traits and trait matching in planktonic predator–prey and host–parasite relationships. *Limnol Oceanogr* 2021;**66**:3857–72. https://doi.org/10.1002/lno.11924.

Llewellyn CA, Fishwick JR, Blackford JC. Phytoplankton community assemblage in the English Channel: a comparison using chlorophyll *a* derived from HPLC-CHEMTAX and carbon derived from microscopy cell counts. *J Plankton Res* 2005;**27**:103–19. https://doi.org/10.1093/plankt/fbh158.

Lønborg C, Middelboe M, Brussaard CPD. Viral lysis of *Micromonas pusilla*: impacts on dissolved organic matter production and composition. *Biogeochemistry* 2013;**116**:231–40. https://doi.org/10.1007/s10533-013-9853-1.

Maat DS, Biggs TEG, Evans C *et al.* Characterization and temperature dependence of Arctic *Micromonas polaris* viruses. *Viruses* 2017;**9**:6–9. https://doi.org/10.3390/v9060134.

Marie D, Partensky F, Vaulot D *et al.* Enumeration of phytoplankton, bacteria, and viruses in marine samples. *Curr Protoc Cytom* 1999;**10**:11.11.1–11.11.15. https://doi.org/10.1002/0471142956.cy1111s10.

Mendes CRB, Tavano VM, Dotto TS *et al.* New insights on the dominance of cryptophytes in Antarctic coastal waters: a case study in Gerlache Strait. *Deep Sea Res Part II Top Stud Oceanogr* 2017;**149**:161–70. https://doi.org/10.1016/j.dsr2.2017.02.010.

Mendes CRB, Tavano VM, Leal MC *et al.* Shifts in the dominance between diatoms and cryptophytes during three late summers in the Bransfield Strait (Antarctic Peninsula). *Polar Biol* 2013;**36**:537–47. https://doi.org/10.1007/s00300-012-1282-4.

Meredith MP, Venables HJ, Clarke A *et al.* The freshwater system west of the Antarctic peninsula: spatial and temporal changes. *J Clim* 2013;**26**:1669–84. https://doi.org/10.1175/JCLI-D-12-00246.1.

Middelboe M. Bacterial growth rate and marine virus-host dynamics. *Microb Ecol* 2000;**40**:114–24. https://doi.org/10.1007/s002480000050.

Mojica KDA, Brussaard CPD. Factors affecting virus dynamics and microbial host—virus interactions in marine environments. *FEMS Microbiol Ecol* 2014;**89**:495–515. https://doi.org/10.1111/1574-6941.12343.

Mojica KDA, Huisman J, Wilhelm SW *et al.* Latitudinal variation in virus-induced mortality of phytoplankton across the North Atlantic Ocean. *ISME J* 2016;**10**:500–13. https://doi.org/10.1038/ismej.2015.130.

Moline MA, Claustre H, Frazer TK *et al.* Alteration of the food web along the Antarctic Peninsula in response to a regional warming trend. *Glob Chang Biol* 2004;**10**:1973–80. https://doi.org/10.1111/j.1365-2486.2004.00825.x.

Moline MA, Prezelin BB, Schofield OM *et al.* Temporal dynamics of coastal Antarctic phytoplankton: environmental driving forces and impact of a 1991/92 summer diatom bloom on the nutrient regimes. In: Battaglia B, Valencia H, Walton DWH (eds), *Antarctic Communities: Species, Structure and Survival*. Cambridge: Cambridge University Press, 1997, 67–72.

Nagasaki K. Dinoflagellates, diatoms, and their viruses. *J Microbiol* 2008;**46**:235–43. https://doi.org/10.1007/s12275-008-0098-y.

Nowicki M, DeVries T, Siegel DA. Quantifying the carbon export and sequestration pathways of the ocean's biological carbon pump. *Global Biogeochem Cycl* 2022;**36**:1–22. https://doi.org/10.1029/2021GB007083.

Pearce I, Davidson AT, Wright S *et al.* Seasonal changes in phytoplankton growth and microzooplankton grazing at an Antarctic coastal site. *Aquat Microb Ecol* 2008;**50**:157–67. https://doi.org/10.3354/ame01149.

Piedade GJ, Wesdorp EM, Montenegro-Borbolla E *et al.* Influence of irradiance and temperature on the virus MpoV-45T infecting the Arctic picophytoplankter *Micromonas polaris*. *Viruses* 2018;**10**:676. https://doi.org/10.3390/v10120676.

R Development Core Team. R: A Language and Environment for Statistical Computing. Vienna: R Foundation for Statistical Computing, 2023.

Rohr T, Long MC, Kavanaugh MT *et al.* Variability in the mechanisms controlling Southern Ocean phytoplankton bloom phenology in an ocean model and satellite observations. *Global Biogeochem Cycl* 2017;**31**:922–40. https://doi.org/10.1002/2016GB005615.

Rose JM, Caron DA. Does low temperature constrain the growth rates of heterotrophic protists? Evidence and implications for algal blooms in cold waters. *Limnol Oceanogr* 2007;**52**:886–95. https://doi.org/10.4319/lo.2007.52.2.0886.

Rose JM, Fitzpatrick E, Wang A *et al.* Low temperature constrains growth rates but not short-term ingestion rates of Antarctic ciliates. *Polar Biol* 2013;**36**:645–59. https://doi.org/10.1007/s00300-013-1291-y.

Rozema PD, Kulk G, Veldhuis MP *et al.* Assessing drivers of coastal primary production in northern Marguerite Bay, Antarctica. *Front Mar Sci* 2017a;**4**:1–20. https://doi.org/10.3389/fmars.2017.00184.

Rozema PD, Venables HJ, van de Poll WH *et al.* Interannual variability in phytoplankton biomass and species composition in northern Marguerite Bay (West Antarctic Peninsula) is governed by both winter sea ice cover and summer stratification. *Limnol Oceanogr* 2017b;**62**:235–52. https://doi.org/10.1002/lno.10391.

Sarker S, Wiltshire KH. Phytoplankton carrying capacity: is this a viable concept for coastal seas?. *Ocean Coast Manag* 2017;**148**:1–8. https://doi.org/10.1016/j.ocecoaman.2017.07.015.

Schofield O, Brown M, Kohut J *et al.* Changes in the upper ocean mixed layer and phytoplankton productivity along the West Antarctic Peninsula. *Philos Trans R Soc A Math Phys Eng Sci* 2018;**376**:20170173. https://doi.org/10.1098/rsta.2017.0173.

Sherr E, Sherr B. Capacity of herbivorous protists to control initiation and development of mass phytoplankton blooms. *Aquat Microb Ecol* 2009;**57**:253–62. https://doi.org/10.3354/ame01358.

Singh BK, Chattopadhyay J, Sinha S. The role of virus infection in a simple phytoplankton zooplankton system. *J Theor Biol* 2004;**231**:153–66. https://doi.org/10.1016/j.jtbi.2004.06.010..

Suttle C. Marine viruses — major players in the global ecosystem. *Nat Rev Microbiol* 2007;**5**:801–12. https://doi.org/10.1038/nrmicro1750.

Thyssen M, Grégori G, Créach V *et al.* Interoperable vocabulary for marine microbial flow cytometry. *Front Mar Sci* 2022;**9**:1–13. https://doi.org/10.3389/fmars.2022.975877.

Van Heukelem L, Thomas CS. Computer-assisted high-performance liquid chromatography method development with applications to the isolation and analysis of phytoplankton pigments. *J Chromatogr A* 2001;**910**:31–49. https://doi.org/10.1016/S0378-4347(00)00603-4.

van Leeuwe MA, Villerius LA, Roggeveld J *et al.* An optimized method for automated analysis of algal pigments by HPLC. *Mar Chem* 2006;**102**:267–75. https://doi.org/10.1016/j.marchem.2006.05.003.

van Leeuwe MA, Webb AL, Venables HJ *et al.* Annual patterns in phytoplankton phenology in Antarctic coastal waters explained by environmental drivers. *Limnol Oceanogr* 2020;**65**:1651–68. https://doi.org/10.1002/lno.11477.

Venables H, Meredith MP, Hendry KR *et al.* Sustained year-round oceanographic measurements from Rothera Research Station, Antarctica, 1997–2017. *Sci Data* 2023;**10**:1–13. https://doi.org/10.1038/s41597-023-02172-5.

Venables HJ, Clarke A, Meredith MP. Wintertime controls on summer stratification and productivity at the Western Antarctic Peninsula. *Limnol Oceanogr* 2013;**58**:1035–47. https://doi.org/10.4319/lo.2013.58.3.1035.

Venables HJ, Meredith MP. Feedbacks between ice cover, ocean stratification, and heat content in Ryder Bay, Western Antarctic Peninsula. *J Geophys Res Ocean* 2014;**119**:5323–36. https://doi.org/10.1002/2013JC009669.

Vernet M, Martinson D, Iannuzzi R *et al.* Primary production within the sea-ice zone west of the Antarctic Peninsula: I—sea ice, summer mixed layer, and irradiance. *Deep Sea Res Part II Top Stud Oceanogr* 2008;**55**:2068–85. https://doi.org/10.1016/j.dsr2.2008.05.021.

Wang X, Smith WO. Phytoplankton growth at low temperatures: results from low temperature incubations. *J Plankton Res* 2021;**43**:633–41. https://doi.org/10.1093/plankt/fbab054.

Weitz JS, Wilhelm SW. Ocean viruses and their effects on microbial communities and biogeochemical cycles. *F1000 Biol Rep* 2012;**4**:17. https://doi.org/10.3410/B4-17.

Worden AZ, Nolan JK, Palenik B. Assessing the dynamics and ecology of marine picophytoplankton: the importance of the eukaryotic component. *Limnol Oceanogr* 2004;**49**:168–79. https://doi.org/10.4319/lo.2004.49.1.0168.

Yamada Y, Tomaru Y, Fukuda H *et al.* Aggregate formation during the viral lysis of a marine diatom. *Front Mar Sci* 2018;**5**. https://doi.org/10.3389/fmars.2018.00167.

Received 28 February 2024; **revised** 26 September 2024; **accepted** 14 February 2025